Two- and three-cluster decays of light nuclei within a hyperspherical harmonics approach

V. S. Vasilevsky,* Yu. A. Lashko,† and G. F. Filippov
Bogolyubov Institute for Theoretical Physics, 14-b Metrolohichna Street, 03143 Kiev, Ukraine

(Received 29 September 2017; revised manuscript received 30 April 2018; published 7 June 2018)

We consider a set of three-cluster systems (^{4}He, ^{7}Li, ^{7}Be, ^{8}Be, ^{10}Be) within a microscopic model which involves hyperspherical harmonics to represent intercluster motion. We selected three-cluster systems which have at least one binary channel. Our aim is to study whether hyperspherical harmonics are able, and under what conditions, to describe two-body channel(s) (nondemocratic motion) or if they are suitable for describing the three-cluster continuum only (democratic motion). It is demonstrated that a rather restricted number of hyperspherical harmonics allows us to describe bound states and scattering states in the two-body continuum for a three-cluster system.

DOI: 10.1103/PhysRevC.97.064605

I. INTRODUCTION

The hyperspherical harmonics (HH) method is a powerful tool for solving many-body problems in different branches of quantum physics, namely atomic, molecular, and nuclear physics. In the orthodox realization of the method, a many-body problem is reduced to a finite or an infinite set of coupled channel problems, representing the many-body Schrödinger equation as a set of coupled one-dimensional differential equations. Efficiency of the method has been repeatedly demonstrated by numerous investigations of few-body problems. Besides, this method has been constantly advanced by creating a more reliable and universal technique for description of the discrete and continuous spectra of many-body systems.

One of the directions in the development of the HH method is to use a full set of oscillator functions, which are labeled by quantum numbers of the hyperspherical harmonics method. We will call them hyperspherical oscillator functions.

In the present paper, we study different channels of decay of three-cluster systems and the ability of the hyperspherical oscillator functions to describe democratic and nondemocratic decay channels. In the literature (see, for instance, Refs. [1–3]) a democratic decay is a synonym for three-body decay or full disintegration of a three-body system. This type of the decay is also called "true" [4] or "truly" [5] three-body scattering. In contrast to the democratic decay, a nondemocratic decay refers to a decay of a compound system into two fragments provided that one of the fragments is represented by a bound state of a two-body subsystem. In what follows we will consider only the dominant three-body configurations of light atomic nuclei. Note that an oscillator basis is a conventional set of functions which are involved in many nuclear models, such as the traditional many-body shell model, the resonating group method, the *ab initio* no-core shell model, and many others.

One of the advantages of the basis of hyperspherical oscillator functions is that it allows one to circumvent the problems enforced by the Pauli principle. The basis simplifies numerical solving of coupled channel differential equations by reducing them to an algebraic matrix form.

Let us consider the following nuclei and appropriate (dominant) three-cluster configurations (3CC), as well as binary decay channels (2CC) (see Table I). In Table I we indicated only those two-cluster decay channels of the three-cluster systems which have a bound state in the corresponding two-cluster subsystem. For instance, for ^{7}Li we take into account channels $\alpha + t$ and $^6\mathrm{Li} + n$, and we omit channel $^5\mathrm{He} + d$ because there are no bound states in the ^{5}He subsystem. In other words, we disregard those binary channels whose threshold energy exceeds the three-cluster threshold. In Table I we also made references to our papers where the corresponding nucleus has been investigated.

We are going to study the eigenspectrum of a microscopic Hamiltonian of the above-mentioned three-cluster systems. For this purpose we will construct matrix elements of the Hamiltonian between many-particle oscillator functions. Diagonalization of the matrix yields eigenvalues and the corresponding eigenfunctions. Some of the obtained eigenvalues represent bound states of the compound system; however, the largest part of the eigenvalues are discretized states in the two- or three-cluster continuum. The number of the eigenvalues and their density in the energy range in question depend on the number of oscillator functions involved in calculation and naturally on the properties of the nucleus under consideration.

To formulate more clearly our aim, let us consider the experimental spectrum of ^{7}Li (see Ref. [9]), one of the nuclei we plan to investigate. In Fig. 1 we display not only the well-known bound and resonance states in ^{7}Li, but also the energy of the lowest two-body decay thresholds ($^4\mathrm{He} + {}^3\mathrm{H}$ and $^6\mathrm{Li} + n$) and one three-body decay threshold ($\alpha + d + n$). Within the present paper we will study if the hyperspherical harmonics are able to reproduce the bound states of ^{7}Li, which have the dominant two-cluster structure $^4\mathrm{He} + {}^3\mathrm{H}$, and how many hyperspherical harmonic have to be involved in

*vsvasilevsky@gmail.com
†ylashko@gmail.com

TABLE I. List of nuclei, their dominant three-cluster configurations, and dominant two-body decay channels.

Nucleus	3CC	2CC 1	2CC 2	2CC 3	Paper
^{4}He	$d+p+n$	^{3}H $+p$	^{3}He $+n$	$d+d$	
^{7}Li	$\alpha+d+n$	$\alpha+t$	^{6}Li $+n$		[6]
^{7}Be	$\alpha+d+p$	$\alpha+^3$He	^{6}Li $+p$		[7]
^{8}Be	$\alpha+^3$H $+p$	^{7}Li $+p$	$\alpha+\alpha$		
^{10}Be	$\alpha+\alpha+2n$	^{6}He $+\alpha$	^{8}Be $+2n$		[8]

calculations to achieve this goal. It is also very interesting to examine whether hyperspherical harmonics allow one to study a continuous spectrum between ^{4}He $+$ ^{3}H and ^{6}Li $+n$ thresholds, and also between two-body ^{6}Li $+n$ and three-body $\alpha+d+n$ thresholds. If so, then what is the required number of hyperspherical harmonics to solve this problem?

The problems we are going to tackle in this paper have been addressed in other ways in [10–13] within the so-called the hyperspherical adiabatic approximation. This approximation works perfectly for a system of three structureless particles and allows one to determine correctly effective potentials for a three-body system and the energies of two- and three-body decay thresholds. However, this approximation is not suitable for three interacting clusters, as the Pauli principle generates nonlocal and energy-dependent potentials.

The method that we employ was formulated in Ref. [14]. It was successfully applied to the study of bound and resonance states of the Borromean nuclei (such as ^{6}He, ^{9}Be, ^{12}C) and resonance states of nuclei with prominent three-cluster features (such as ^{5}H, ^{6}Be, ^{9}B). All these nuclei were considered as three-cluster systems. The present paper may be considered as a step forward in creating a unified microscopic model for describing both binary and three-cluster channels.

In this paper we will study wave functions of the deeply- and weakly-bound states with respect to two- and three-cluster thresholds. For the weakly bound states, we will demonstrate that a binary structure is revealed in the three-cluster wave function of the pseudobound states whose energy is close to the corresponding binary decay threshold. Despite the fact that to obtain convergent results for the energies of resonance states lying between the lowest binary decay threshold and three-cluster decay threshold of a three-cluster system one needs a large basis of hyperspherical harmonics, it is possible to see the evidence of two-cluster structure in the three-cluster wave function of a pseudobound state, but with a rather restricted set of hyperspherical harmonics.

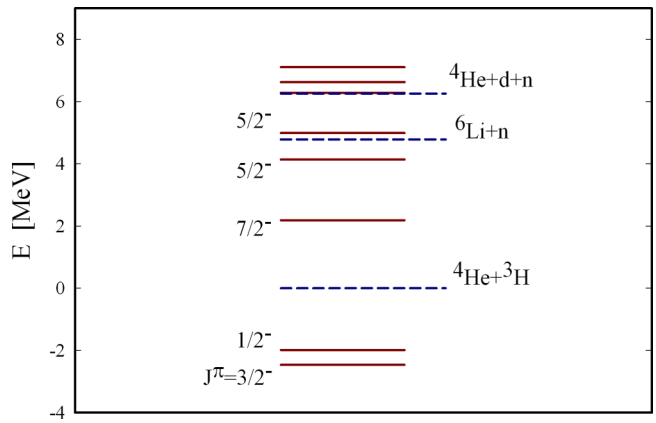

FIG. 1. Experimental spectrum of ^{7}Li.

This article is organized as follows. In Sec. II we present a brief review of a microscopic three-cluster model which exploits the hyperspherical harmonics. For this model we will use an abbreviation AMHHB which means the algebraic model of three-cluster systems involved the hyperspherical harmonics basis. The focus of this section is the asymptotic form of three-cluster wave functions describing two- and three-cluster decay of a compound system. In Sec. III, we analyze convergence of the spectrum of three-cluster systems and study peculiarities of wave functions of bound and pseudobound states in different asymptotic regimes. Brief conclusions are presented in Sec. IV.

II. METHOD

First of all we need to introduce coordinates which determine relative position of clusters in coordinate space. The most suitable variables we believe are the Jacobi vectors $\mathbf{x}$ and $\mathbf{y}$. One can introduce three different sets (or different trees) of Jacobi vectors. Within the Faddeev formalism for three particles or within coupled channel formalism for three clusters, one has to use all three sets of Jacobi vectors. In what follows we stick to one tree of the Jacobi vectors. We will discuss latter why only one set of the Jacobi vectors is sufficient for our purposes in the hyperspherical harmonics formalism.

We start the model formulation with an explicit form of wave function for a system consisting of three s clusters:

$$\Psi_{E,LM_L} = \widehat{\mathcal{A}}\{\Phi_1(A_1)\Phi_2(A_2)\Phi_3(A_3)\psi_{E,LM_L}(\mathbf{x},\mathbf{y})\}. \quad (1)$$

This is a traditional form of a wave function of the resonating group method for systems, when at least one cluster consists of two or more nucleons. The internal structure of clusters ($\alpha = 1,2,3$) is described by the antisymmetric and translationally invariant wave functions $\Phi_\alpha(A_\alpha)$. Function $\Phi_\alpha(A_\alpha)$ is a wave function of the many-particle shell model with the most compact configuration of nucleons. These functions are selected in such a way as to provide in the most economical manner a fairly good description of the main internal properties (bound-state energy, cluster size) of each cluster. The antisymmetrization operator $\widehat{\mathcal{A}}$ makes antisymmetric the wave function of the compound three-cluster system, which is of paramount importance for the energy region under consideration. Since all functions $\Phi_\alpha(A_\alpha)$ are fixed, to calculate a spectrum and wave functions of the compound system one has to determine a wave function of intercluster motion $\psi_{LM_L}(\mathbf{x},\mathbf{y})$. This function is also translationally invariant and depends on two Jacobi vectors $\mathbf{x}$ and $\mathbf{y}$, locating relative positions of clusters in the space. By using angular orbital momentum reduction, we represent this function as an infinite series,

$$\psi_{E,LM_L}(\mathbf{x},\mathbf{y}) \Rightarrow \sum_{\lambda,l} \psi_{E;\lambda,l;L}(x,y)\{Y_\lambda(\widehat{\boldsymbol{x}})Y_l(\widehat{\boldsymbol{y}})\}_{LM_L}, \quad (2)$$

where $\widehat{\boldsymbol{x}}$ and $\widehat{\boldsymbol{y}}$ are unit vectors, and λ and l are the partial angular momenta associated with vectors $\mathbf{x}$ and $\mathbf{y}$ respectively.

Note that the form of Eq. (1) implies that the total orbital momentum L is a good quantum number. It also means that

in what follows we disregard the noncentral components of nucleon-nucleon interaction (for the sake of simplicity).

A. Hyperspherical coordinates and basis

Wave functions of intercluster motion $\psi_{\lambda,l;L}(x,y)$ obey an infinite set of the two-dimension (in terms of variables x and y) integro-differential equations. To solve such equations we make use of the hyperspherical coordinates and hyperspherical harmonics. There are several schemes for introducing hyperspherical coordinates or, more exactly, hyperspherical angles Ω_5, as hyperspherical radius is determined uniquely. Each choice of the hyperspherical angles invokes a certain set of five quantum numbers enumerating hyperspherical harmonics. Different sets of the hyperspherical angles, however, have three common quantum numbers: the hypermomentum K, the total orbital momentum L, and its projection M_L on the z axis.

We make use of the hyperspherical harmonics in the form suggested by Zernike and Brinkman in Ref. [15], because this form is very simple, it does not involve bulky calculations, and the quantum numbers have clear physical meaning. To introduce the Zernike-Brinkman hyperspherical harmonics, we need to determine the hyperspherical coordinates. Instead of six variables $\mathbf{x}$ and $\mathbf{y}$ or x, y, and two unit vectors $\widehat{\boldsymbol{x}}$ and $\widehat{\boldsymbol{y}}$, we introduce a hyperspherical radius

$$\rho = \sqrt{x^2 + y^2} \tag{3}$$

and a hyperspherical angle

$$\theta = \arctan\left(\frac{x}{y}\right).$$

At a given value of ρ, this angle determines relative length of the vectors $\mathbf{x}$ and $\mathbf{y}$:

$$x = \rho\cos\theta, \quad y = \rho\sin\theta, \quad \theta \in [0,\pi/2]. \tag{4}$$

For small values of θ, the length of vector y is close to zero, and vector x has maximal value $x \approx \rho$. When the hyperspherical angle θ is close to $\pi/2$, the length of vector x is very small and vector y is at its maximum.

The represented set of the hyperspherical angles is a very popular scheme of using hyperspherical coordinates for investigating three-body [16–18], and three-cluster systems [14,19–21].

In new coordinates

$$\psi_{E,LM_L} \Rightarrow \sum_c \phi_{E,c}(\rho)\mathcal{Y}_c(\Omega_5), \tag{5}$$

where $\mathcal{Y}_c(\Omega_5)$ stands for the product

$$\mathcal{Y}_c(\Omega_5) = \chi_K^{(\lambda,l)}(\theta)\{Y_\lambda(\widehat{\boldsymbol{x}})Y_l(\widehat{\boldsymbol{y}})\}_{LM_L} \tag{6}$$

and represents a hyperspherical harmonic for a three-cluster channel

$$c = \{K,\lambda,l,L\}. \tag{7}$$

The hyperspherical harmonic $Y_c(\Omega_5)$ is a function of five angular variables $\theta,\theta_1,\phi_1,\theta_2,\phi_2$. Definitions of all components of the hyperspherical harmonic $Y_c(\Omega_5)$ can be found, for instance, in Ref. [14]. Being a complete basis, the hyperspherical harmonics account for any shape of the three-cluster triangle and its orientation. Thus they account for all possible modes of relative motion of three interacting clusters.

As for the hyperradial wave functions $\phi_{E,c}(\rho)$, they obey a system of differential equations with local effective potentials for three structureless particles, or a set of integro-differential equations with nonlocal effective potentials for three clusters. The latter can be represented as

$$\sum_{\widetilde{c}}\left[\delta_{c,\widetilde{c}}\widehat{T}_K\phi_{E,c}(\rho) + \int d\widetilde{\rho}\widetilde{\rho}^5 V_{c,\widetilde{c}}(\rho,\widetilde{\rho})\phi_{E,\widetilde{c}}(\widetilde{\rho})\right] = E\sum_{\widetilde{c}}\int d\widetilde{\rho}\widetilde{\rho}^5\mathcal{N}_{c,\widetilde{c}}(\rho,\widetilde{\rho})\phi_{E,\widetilde{c}}(\widetilde{\rho}), \tag{8}$$

where $\mathcal{N}_{c,\widetilde{c}}(\rho,\widetilde{\rho})$ is a norm kernel and

$$\widehat{T}_K = -\frac{\hbar^2}{2m}\left[\frac{\partial^2}{\partial\rho^2} + \frac{5}{\rho}\frac{\partial}{\partial\rho} - \frac{K(K+4)}{\rho^2}\right]. \tag{9}$$

As one can see, the Pauli principle leads to appearance of the energy-dependent part in the effective potential [the right-hand side of Eqs. (8). To simplify solving the set of equations (8), we invoke a full set of oscillator functions to expand the sought wave function

$$\psi_{E,LM_L} = \sum_{n_\rho,c} C_{E;n_\rho,c}|n_\rho,c\rangle.$$

This reduces the set of integro-differential equations (8) to an algebraic form, i.e., to the system of linear algebraic equations

$$\sum_{\widetilde{n}_\rho,\widetilde{c}}[\langle n_\rho,c|\mathcal{H}_{c,\widetilde{c}}|\widetilde{n}_\rho,\widetilde{c}\rangle - E\langle n_\rho,c|\mathcal{N}_{c,\widetilde{c}}|\widetilde{n}_\rho,\widetilde{c}\rangle]C_{E,\widetilde{n}_\rho,\widetilde{c}} = 0, \tag{10}$$

where $\mathcal{H}_{c,\widetilde{c}}$ is a Hamiltonian kernel:

$$\mathcal{H}_{c,\widetilde{c}} = \mathcal{H}_{c,\widetilde{c}}(\rho,\widetilde{\rho}) = \delta_{c,\widetilde{c}}\widehat{T}_K\delta(\rho-\widetilde{\rho}) + V_{c,\widetilde{c}}(\rho,\widetilde{\rho}).$$

Oscillator functions for three-cluster configuration are determined as

$$|n_\rho,c\rangle = |n_\rho,K;\lambda,l;L\rangle = R_{n_\rho K}(\rho,b)\mathcal{Y}_c(\Omega_5), \tag{11}$$

where $R_{n_\rho,K}(\rho,b)$ is an oscillator function,

$$R_{n_\rho,K}(\rho,b) = (-1)^{n_\rho}\mathcal{N}_{n_\rho,K}r^K\exp\left\{-\frac{1}{2}r^2\right\}L_{n_\rho}^{K+3}(r^2),$$
$$r = \rho/b, \quad \mathcal{N}_{n_\rho,K} = b^{-3}\sqrt{\frac{2\Gamma(n_\rho+1)}{\Gamma(n_\rho+K+3)}}, \tag{12}$$

and b is an oscillator length.

The system of equations (10) can be solved numerically by imposing restrictions on the number of hyperradial excitations n_ρ and on the number of hyperspherical channels $c_1,c_2,\ldots,c_{N_{ch}}$. The diagonalization procedure may be used to determine energies and wave functions of the bound states. However, the proper boundary conditions have to be implemented to calculate elements of the scattering S matrix and corresponding functions of continuous spectrum. Boundary conditions or asymptotic behavior of wave functions for democratic and nondemocratic decay of a compound three-cluster system will be considered in Sec. II C.

Wave function (11) belongs to the oscillator shell with the number of oscillator quanta $N_{\rm os} = 2n_\rho + K$. It is convenient to numerate the oscillator shells by $N_{\rm sh}$ $(= 0,1,2,\ldots)$, which we determine as

$$N_{\rm os} = 2n_\rho + K = 2N_{\rm sh} + K_{\rm min},$$

where $K_{\rm min} = L$ for normal parity states $\pi = (-1)^L$ and $K_{\rm min} = L + 1$ for abnormal parity states $\pi = (-1)^{L+1}$. Thus we account for oscillator shells starting from a "vacuum" shell ($N_{\rm sh} = 0$) with minimal value of the hypermomentum $K_{\rm min}$ compatible with a given total orbital momentum L.

It is worth noticing that Eq. (10) contains the norm kernel matrix $\|\langle n_\rho,c|\mathcal{N}_{c,\tilde{c}}|\tilde{n}_\rho,\tilde{c}\rangle\|$, which is also called the matrix of the antisymmetrization operator. Appearance of this matrix in the equation means that the oscillator basis functions (11) are not orthonormal due to the Pauli principle. Moreover, these functions may be linearly dependent, which leads to appearance of the Pauli forbidden states. This problem has been addressed several times; see, for example, Refs. [22,23].

Existence of the Pauli forbidden states requires the system of equations (10) to be solved in two steps. In the first step, one needs to diagonalize the norm kernel matrix $\|\langle n_\rho,c|\mathcal{N}_{c,\tilde{c}}|\tilde{n}_\rho,\tilde{c}\rangle\|$. This matrix has a block structure. Matrix $\|\langle n_\rho,c|\mathcal{N}_{c,\tilde{c}}|\tilde{n}_\rho,\tilde{c}\rangle\|$ has a very large number of zero matrix elements. Nonvanishing matrix elements of this matrix are overlaps of basis functions of the same oscillator shell. This statement can be expressed as the following condition:

$$2n_\rho + K = 2\tilde{n}_\rho + \tilde{K}$$

Such block structure of the overlap matrix significantly simplifies calculations of its eigenstates $\Lambda_{N_{\rm sh},\alpha}$ $(\alpha = 1,2,\ldots)$ and corresponding eigenfunctions $O^{N_{\rm sh},\alpha}_{n_\rho,c}$. These eigenfunctions form an orthogonal matrix which transform the original basis functions $|n_\rho,c\rangle$ to a new set of functions

$$|N_{\rm sh},\alpha\rangle = \sum_{n_\rho,c\in N_{\rm sh}} O^{N_{\rm sh},\alpha}_{n_\rho,c}|n_\rho,c\rangle.$$

We check whether a particular eigenvalue $\Lambda_{N_{\rm sh},\alpha}$ equals zero. If so, this eigenvalue is the Pauli forbidden state and has to be eliminated from our Hilbert space. Otherwise, this eigenstate belongs to the part of the total three-cluster Hilbert space spanned by the Pauli allowed states. The first stage of solving a set of Eqs. (10) is completed by constructing the normalized Pauli allowed states $|N_{\rm sh},c_a\rangle = |N_{\rm sh},\alpha\rangle/\sqrt{\Lambda_{N_{\rm sh},\alpha}}$, where index c_a numerates the Pauli allowed states on the oscillator shell $N_{\rm sh}$.

In the second step, one needs to transform the matrix of the Hamiltonian from the original basis of functions $|n_\rho,c\rangle$ to the basis of the normalized Pauli allowed states $|N_{\rm sh},c_a\rangle$.

For numerical solution of Eq. (10) one has to construct matrix elements of a microscopic Hamiltonian with a selected nucleon-nucleon potential and the norm kernel matrix. We do not dwell on this problem since the appropriate method of constructing such matrices was formulated in Ref. [14].

B. Strategy of investigation

To achieve the goals formulated above we carry out our investigations in the following steps:

(1) We calculate matrix elements of a Hamiltonian between three-cluster oscillator functions
(2) By solving an eigenvalue problem, we obtain the spectrum of bound and pseudobound states, and the corresponding wave functions in discrete representation.
(3) To study the nature of the obtained solutions, we construct correlation functions and calculate the weight of different oscillator shells in wave functions of bound and pseudobound states
(4) Finally, we analyze the structure of the wave functions in discrete and coordinate representations and study their asymptotic behavior.

Some remarks should be made to explain and justify this strategy. First, such a way of investigating a three-cluster system allows us to avoid the application of the necessary boundary conditions which leads to very bulky and time-consuming calculations. The diagonalization procedure enables us in a rather simple way to obtain wave functions of bound and scattering states in the internal region where effects of cluster-cluster interaction are very strong. By increasing the number of oscillator functions we obtain a more correct description of the bound states, gradually approaching the exact value of the energy and the correct shape of a wave function, mainly improving its asymptotic tail.

Meanwhile, we have a different situation for continuous spectrum states. The extension of the oscillator basis allows one to scan the continuous spectrum and to study the internal part of wave functions for different energies of the spectrum. The internal part of wave functions represents the exact wave function with a specific "boundary condition." This will be later discussed in more detail. Concluding, we note that the digonalization procedure of a huge but restricted Hamiltonian matrix is very often used to study spectra of light nuclei with the *ab initio* no-core shell model.

C. Asymptotic behavior of the wave functions

Let us consider an asymptotic behavior of wave function (1). It is more appropriate to introduce an analog of the Faddeev amplitudes $\psi^{(\alpha)}_L(\mathbf{x}_\alpha,\mathbf{y}_\alpha)$,

$$\begin{aligned}\Psi_{E,LM_L} &= \sum_{\alpha=1}^{3}\widehat{\mathcal{A}}\big\{\Phi_1(A_1)\Phi_2(A_2)\Phi_3(A_3)\psi^{(\alpha)}_{E,LM_L}(\mathbf{x}_\alpha,\mathbf{y}_\alpha)\big\}\\ &= \sum_{\alpha=1}^{3}\sum_{\lambda_\alpha,l_\alpha}\widehat{\mathcal{A}}\big\{\Phi_1(A_1)\Phi_2(A_2)\Phi_3(A_3)\\ &\quad\times\psi^{(\alpha)}_{E,\lambda_\alpha,l_\alpha;L}(x_\alpha,y_\alpha)\{Y_{\lambda_\alpha}(\widehat{\mathbf{x}}_\alpha)Y_{l_\alpha}(\widehat{\mathbf{y}}_\alpha)\}_{LM_L}\big\},\end{aligned} \quad (13)$$

to study the asymptotic properties of three-cluster systems. In Eq. (13), $\mathbf{x}_\alpha$ is the Jacobi vector, determining the distance between β and γ clusters, while $\mathbf{y}_\alpha$ is a Jacobi vector linking

the αth cluster with the center of mass of the β and γ clusters:

$$\mathbf{x}_\alpha = \sqrt{\frac{A_\beta A_\gamma}{A_\beta + A_\gamma}}(\mathbf{R}_\beta - \mathbf{R}_\gamma), \tag{14}$$

$$\mathbf{y}_\alpha = \sqrt{\frac{A_\alpha(A_\beta + A_\gamma)}{A_\alpha + A_\beta + A_\gamma}}\left[\mathbf{R}_\alpha - \frac{A_\beta \mathbf{R}_\beta + A_\gamma \mathbf{R}_\gamma}{A_\beta + A_\gamma}\right],$$

$$\mathbf{R}_\sigma = \frac{1}{A_\sigma}\sum_{i\in A_\sigma} \mathbf{r}_i. \tag{15}$$

The indexes α, β, and γ form a cyclic permutation of 1, 2, and 3.

In general, there are four different asymptotic regions in a three-cluster system. The asymptotic properties of three-body functions in these regions are thoroughly discussed in Refs. [24–26]. We follow notations of Ref. [25] (see pages 134–136) and denote these asymptotic regions as Ω_α ($\alpha = 1,2,3$) and Ω_0. In the asymptotic regions Ω_α the distance between clusters with indexes β and γ is much smaller than the distance of the third cluster (with index α) to the center of mass of clusters β and γ ($|\mathbf{x}_\alpha| \ll |\mathbf{y}_\alpha|$). This region describes scattering of a cluster with index α on a bound state of clusters β and γ. The asymptotic region Ω_0 describes the situation when all clusters are well separated, i.e., when intercluster distances $|\mathbf{x}_\alpha| \gg a$ ($\alpha = 1,2,3$) are larger then the radius a of a short-range interaction.

Consider the asymptotic region Ω_α. In this region, the Faddeev amplitude $\psi^{(\alpha)}_{E,L}(\mathbf{x}_\alpha,\mathbf{y}_\alpha)$ has the following "two-body" asymptotic form:

$$\psi^{(\alpha)}_{E,\lambda_\alpha,l_\alpha;L}(x_\alpha,y_\alpha) \approx \sum_{\lambda_\alpha,l_\alpha} g_{\lambda_\alpha,\mathcal{E}_\alpha}(x_\alpha)\left[\delta_{c_0,c}\,\psi^{(-)}_{k_\alpha,l_\alpha}(k_\alpha y_\alpha) - S_{c_0,c}\,\psi^{(+)}_{k_\alpha,l_\alpha}(k_\alpha y_\alpha)\right] \tag{16}$$

for scattering states (when the total energy $E \geqslant \mathcal{E}_\alpha$) and

$$\begin{aligned}\psi^{(\alpha)}_{E,\lambda_\alpha,l_\alpha;L}(x_\alpha,y_\alpha) &\approx \sum_{\lambda_\alpha,l_\alpha} A_{c_0,c} g_{\lambda_\alpha,\mathcal{E}_\alpha}(x_\alpha) W_{-\eta_\alpha,l_\alpha+1/2}(2k_\alpha y_\alpha)\\ &\approx \sum_{\lambda_\alpha,l_\alpha} A_{c_0,c} g_{\lambda_\alpha,\mathcal{E}_\alpha}(x_\alpha)\frac{1}{(\kappa_\alpha y_\alpha)^{\eta_\alpha+1}}\exp\{-\kappa_\alpha y_\alpha\}\end{aligned} \tag{17}$$

for bound states (when the total energy $E < \mathcal{E}_\alpha$). Here $\psi^{(-)}_{k_\alpha,l_\alpha}(k_\alpha y_\alpha)$ and $\psi^{(+)}_{k_\alpha,l_\alpha}(k_\alpha y_\alpha)$ are incoming and outgoing waves, respectively, determined in terms of the well-known regular $F_{l_\alpha}(k_\alpha y_\alpha;\eta_\alpha)$ and irregular $G_{l_\alpha}(k_\alpha y_\alpha;\eta_\alpha)$ Coulomb functions:

$$\begin{aligned}\psi^{(\pm)}_{k_\alpha,l_\alpha}(k_\alpha y_\alpha) &= \left[G_{l_\alpha}(k_\alpha y_\alpha;\eta_\alpha) \pm F_{l_\alpha}(k_\alpha y_\alpha;\eta_\alpha)\right]/y_\alpha\\ &\underset{y_\alpha\to\infty}{\approx} \exp\left\{\pm i\left(k_\alpha y_\alpha - l_\alpha\frac{\pi}{2} - \eta_\alpha \ln(2k_\alpha y_\alpha) + \sigma_{l_\alpha}\right)\right\}/y_\alpha,\end{aligned} \tag{18}$$

and $W_{-\eta_\alpha,l_\alpha+1/2}(2k_\alpha y_\alpha)$ is the Whittaker function. In Eqs. (16) and (17), index $c = \{\lambda_\alpha,\mathcal{E}_\alpha,l_\alpha\}$ enumerates the current channel, c_0 indicates the incoming channel, $\mathcal{E}_\alpha$ and $g_{\lambda_\alpha,\mathcal{E}_\alpha}(x_\alpha)$ denote energy of the two-cluster bound state and its wave function, and

$$k_\alpha = \sqrt{\frac{2m(E-\mathcal{E}_\alpha)}{\hbar^2}}, \quad \kappa_\alpha = \sqrt{\frac{2m|E-\mathcal{E}_\alpha|}{\hbar^2}}, \tag{19}$$

$$\eta_\alpha = \frac{Z_\alpha(Z_\beta+Z_\gamma)e^2}{\sqrt{|E-\mathcal{E}_\alpha|}}\sqrt{\frac{A_\alpha(A_\beta+A_\gamma)}{A}\frac{m}{\hbar^2}}. \tag{20}$$

Let us turn our attention to the asymptotic region Ω_0. We present an asymptotic form only for neutral clusters (or by neglecting the Coulomb interaction in asymptotic region). In this case an asymptotic form of the three-cluster wave function is well and unambiguously established. For a bound state of the three-cluster system the wave function $\psi^{(\alpha)}_{E,\lambda_\alpha,l_\alpha;L}(x_\alpha,y_\alpha)$ is

$$\psi^{(\alpha)}_{E,\lambda_\alpha,l_\alpha;L}(x_\alpha,y_\alpha) = \psi^{(\alpha)}_{\lambda_\alpha,l_\alpha;L}(\rho,\theta_\alpha) \approx \exp\{-\kappa_0\,\rho\}/\rho^{5/2}, \tag{21}$$

and for a scattering state (full disintegration or breakup)

$$\begin{aligned}\psi^{(\alpha)}_{E,\lambda_\alpha,l_\alpha;L}(x_\alpha,y_\alpha) &= \psi^{(\alpha)}_{\lambda_\alpha,l_\alpha;L}(\rho,\theta_\alpha)\\ &\approx A_{c_0,c}(\theta_\alpha)\exp\{ik_0\,\rho\}/\rho^{5/2},\end{aligned} \tag{22}$$

where $A_{c_0,c}(\theta_\alpha)$ is a breakup amplitude and

$$k_0 = \sqrt{\frac{2m(E-\mathcal{E}_0)}{\hbar^2}}, \quad \kappa_0 = \sqrt{\frac{2m|E-\mathcal{E}_0|}{\hbar^2}};$$

$\mathcal{E}_0$ is the three-cluster threshold energy.

As we see, the hyperspherical coordinates are involved to express an asymptotic form of wave functions for the democratic decay of a three-cluster system or its bound state [see Eqs. (21) and (22)]. They can be also used to express an asymptotic behavior of three-cluster wave functions in all asymptotic regions by using relations (4).

So far, we have discussed the asymptotic behavior of three-cluster wave functions for different scenarios of two- and three-body decays in coordinate representations. Similar relations can be written in a discrete representation by using the correspondence between the expansion coefficients and the wave functions in coordinate space.

Let us assume that we arranged all binary channels in such an order that $\mathcal{E}_1 < \mathcal{E}_2 < \mathcal{E}_3$. We also assume that all energies are measured from the three-cluster threshold and thus $\mathcal{E}_0 = 0$. With such definitions, an asymptotic part of bound-state wave functions will be mainly represented by the wave function from Eq. of the first channel (17). Contributions of other binary channels and the three-cluster channel depend on how far this state is from the corresponding decay threshold as well. The larger is the difference $|E-\mathcal{E}_\sigma|$ ($\sigma = 0,1,2,3$), the smaller is the contribution of the corresponding channel to the asymptotic part of the bound-state wave function. It is obvious that to obtain the deeply bound state (with respect to the three-cluster threshold), a very small number of hyperspherical harmonics is required. For a weakly bound state, a large number of hyperspherical harmonics should be involved to reach a necessary precision for the energy of this state. The wave function of a continuous spectrum state with energy $\mathcal{E}_1 < E < \mathcal{E}_2$ is expected to be mainly represented by the

wave function of the first channel of the form (16). When the energy of this state approaches the energy of the second binary channels, it is natural to expect a substantial contribution of the second closed channel. A more intriguing situation can be observed for continuous spectrum states when two binary channels are open, i.e., for the states with energy $\mathcal{E}_2 < E < \mathcal{E}_3$. The wave function of such state can be represented either by the first or by the second channels, or by a combination of both channels. More complicated situations can be observed for continuous spectrum states when all binary channels are open ($\mathcal{E}_3 < E < 0$).

D. Oscillator basis

Note that the first two steps in the strategy mentioned in Sec. II B are common for many microscopic and semimicroscopic model calculations, since many models used a square-integrable basis to obtain information about bound and scattering states. The oscillator basis is the most used one among others. Two main merits of this basis make it popular. First, these basis functions are orthonormal: they do not create any problem with overfullness or linear dependence of basis functions. Second, due to the specific properties of oscillator functions, there is a simple relationship between expansion coefficients and an original wave function. It makes more transparent the physical interpretation of the obtained results.

Now we consider other two advantages of the basis which will be exploited in what follows. First, the oscillator basis allows one to implement correct boundary conditions in a discrete oscillator representation [27,28]. Second, diagonalization of a matrix of a microscopic Hamiltonian, constructed with the oscillator basis, reveals eigenfunctions with clear physical properties. To explain the second advantage of the oscillator basis we consider a single-channel approximation for a two-cluster or two-body system. Suppose we construct the matrix elements of Hamiltonian $\widehat{H}$ between oscillator functions $|n\rangle$ and $|m\rangle$. By diagonalizing matrix $\|\langle n|\widehat{H}|m\rangle\|$ with dimension $N \times N$, we obtain eigenvalues E_ν ($\nu = 0,1,2,\ldots,N-1$) and the corresponding eigenfunctions $\{C_n^{(\nu)}\}$. Eigenvalues E_α represent bound states if $E_\nu < 0$, and pseudobound states for positive energy $E_\nu > 0$. It was shown in Refs. [29–31], that pseudobound states are the states of continuous spectrum states selected from an infinite set through the diagonalization procedure by the condition $C_{N+1}^{(\nu)} = 0$. In other words, these states have a node at a given point. This condition can be also used to determine phase shifts at these discrete points. An interesting feature of the pseudobound states is that without imposing any boundary condition one can obtain a set of *discrete* or selected states in the two-cluster continuum. A very important feature of the pseudo-bound states is that the wave function of a pseudo-bound state coincides (within a factor) with the properly normalized wave function of the continuous spectrum with the same energy.

To confirm the aforementioned properties of wave functions in the oscillator representation, we show the following illustration. In Fig. 2 we display eigenfunctions of the two-cluster $\alpha + t$ Hamiltonian for the $3/2^-$ state in ^{7}Li. These

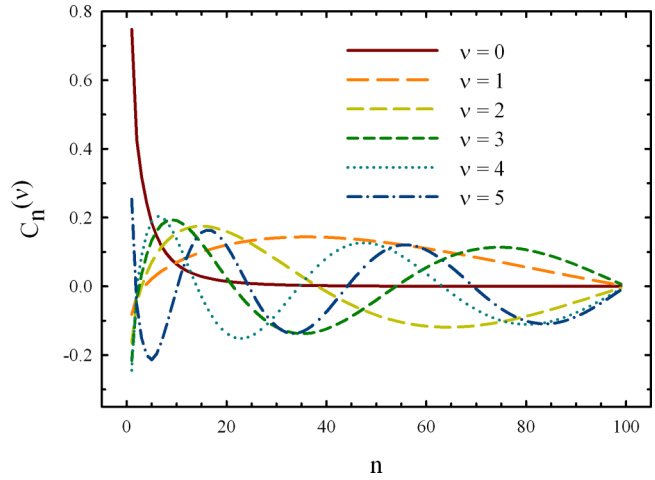

FIG. 2. Six eigenfunctions of the $3/2^-$ state in ^{7}Li obtained in the two-cluster $\alpha + t$ approximation.

functions are determined with 100 oscillator functions. The first eigenfunction describes the ^{7}Li ground state; the other five functions represent states of the two-cluster continuum. One can see explicitly that the wave functions of these states indeed have a node at the end of an interval $n = N + 1$. The same is true for the ground state; however, it is not so evident in Fig. 2. We do not dwell on the details of such calculations, as they can be found, for instance, in Ref. [8].

To prove briefly that eigenstates of a two-cluster Hamiltonian have clear physical meaning, we consider wave functions of four $3/2^-$ pseudobound states in ^{7}Li. These state are obtained with different numbers N of oscillator functions. We selected and displayed in Fig. 3 those pseudobound states which have approximately the same energy. Thus one can expect that wave functions of these states have the same structure (shape). Indeed, we see that the selected wave functions have maxima and nodes at the same points of the discrete space.

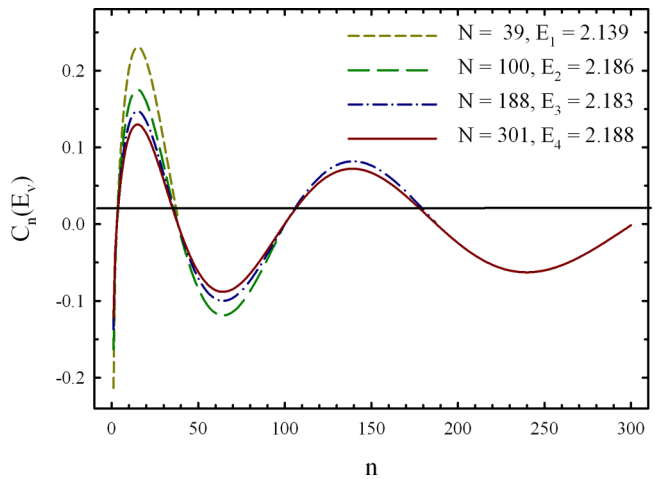

FIG. 3. Wave functions of the $3/2^-$ pseudobound states in ^{7}Li = $\alpha + t$ obtained for approximately the same energy and with different numbers of oscillator functions.

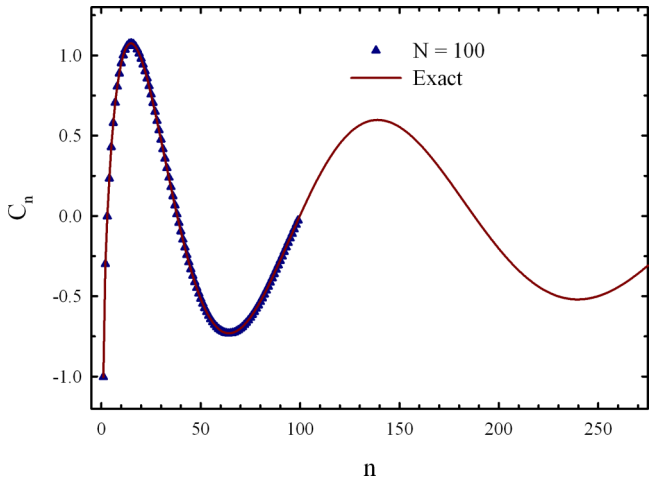

FIG. 4. The exact wave function of the $3/2^-$ state of $^7\mathrm{Li} = \alpha + t$ with energy $E = 2.186$ MeV compared with the renormalized wave function of the pseudobound state, obtained for the same energy and with 100 oscillator functions.

They differ only by the normalization condition

$$\sum_{n=0}^{N} \left|C_n^{(\nu)}\right|^2 = 1$$

and represent the corresponding state in different oscillator spaces $0 \leqslant \nu \leqslant N$ ($N = 39,100,188,301$). In Fig. 3 we indicate the number of the displayed eigenstate ν and its energy E_ν. If we normalize four wave functions in the same fashion (for instance, as the wave function with the minimal value of oscillator functions $N = 39$), we will obtain four quite close wave functions in the interval $0 \leqslant \nu \leqslant 39$, three quite close functions in the interval $0 \leqslant \nu \leqslant 100$, and two quite close wave functions in the interval $0 \leqslant \nu \leqslant 188$. Note that these wave functions, obtained with the diagonalization procedure, coincide within a simple normalization factor with the exact wave function of the continuous spectrum state obtained for the same energy and with the corresponding boundary conditions. This is demonstrated in Fig. 4, where we display the exact wave function, obtained for the energy $E = 2.186$ MeV by imposing the correct boundary condition, and the renormalized wave function, determined for the same energy with 100 oscillator functions. One can see that both exact and approximate functions coincide in the range $0 \leqslant n \leqslant 100$. It is important to note that the exact wave function is determined in the whole oscillator space ($0 \leqslant n < \infty$) and normalized by the condition

$$\sum_{n=0}^{\infty} C_n^{(E)*} C_n^{(\tilde{E})} = \delta(E - \tilde{E}).$$

To this end, yet another visual confirmation that the diagonalization procedure reveals states with clear physical meaning is presented in Ref. [31]. Figure 1 (p. 714) of Ref. [31] demonstrates an approximation of the wave function of the continuum spectrum by expansion in the discrete basis with different numbers of basis functions. The above-mentioned figure clearly shows that the larger is the number of basis functions involved, the larger is the region of good approximation of the exact wave function by partial sum. However, the behavior of the wave function in the inner region is well reproduced even with a rather restricted set of basis functions.

Thereby, the wave functions obtained by the diagonalization of the Hamiltonian have the same physical meaning as the wave functions obtained with the proper boundary conditions. The only difference is that the former are known only up to a finite point of coordinate space, while the latter are known in the whole region.

We will not dwell on this subject, as more details on J-matrix methods can be found in the book of articles [32].

It is also important to note that the methods which use the oscillator basis are similar to the well-known R-matrix model of nuclear reactions. In these methods eigenvalues E_ν and eigenfunctions $\{C_n^{(\nu)}\}$ are important blocks for construction of the elements of the scattering matrix and wave functions of single- and many-channel systems for an arbitrary value of the energy E. The explicit formulas relating elements of the S matrix with eigenvalues E_ν and eigenfunctions $\{C_n^{(\nu)}\}$ can be found in Refs. [29,33]. In Refs. [34,35], these formulas were extended to the case of many-channel systems described with the hyperspherical basis. Besides, investigations of eigenvalues E_ν and eigenfunctions $\{C_n^{(\nu)}\}$ can be considered as a simple case of the complex scaling method (see basic definitions of the method and its recent progress in applications to many-cluster systems in Refs. [36,37]), when the rotational angle equals zero.

III. RESULTS AND DISCUSSION

We involve the Minnesota potential (MP) [38,39] as a nucleon-nucleon potential in our calculations. We use a common oscillator length for all clusters. Its value is selected to minimize the energy of the three-cluster threshold. To construct a wave function of two-cluster relative motion and to determine the energy of a two-cluster bound state, we employ the oscillator basis. Details of two-cluster calculations can be found in Ref. [8]. We make use of 50 oscillator functions to calculate the ground-state energies of two-cluster systems. This number of functions provides the correct value of bound-state energies and their parameters (for instance, rms proton and mass radii, and so on).

In Table II we show input parameters of our calculations. They include oscillator length b and exchange parameters u of the selected NN potential.

TABLE II. Input parameters of calculations for each nucleus.

Nucleus	3CC	b (fm)	u
^{4}He	$d + (p + n)$	1.489	0.9600
^{7}Li	$\alpha + d + n$	1.311	0.9255
^{7}Be	$\alpha + d + p$	1.311	0.9255
^{8}Be	$\alpha + {}^3\mathrm{H} + p$	1.311	0.9560
^{10}Be	$\alpha + \alpha + 2n$	1.356	0.9570

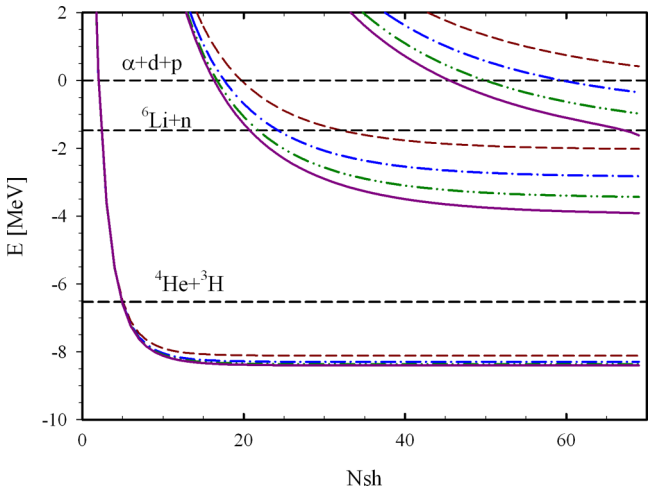

FIG. 5. Spectrum of the $3/2^-$ states in ^{7}Li as a function of $N_{\rm sh}$ and $K_{\rm max}$. Dashed line: $K_{\rm max} = 7$; dot-dashed line: $K_{\rm max} = 9$; dot-dot-dashed line: $K_{\rm max} = 11$; and solid line: $K_{\rm max} = 13$.

As in Refs. [40–43], in the present paper we will vary the hyperspherical momentum in the range $L \leqslant K \leqslant K_{\rm max}$, where $K_{\rm max} = 14$ for the positive parity states and $K_{\rm max} = 13$ for the negative parity states. The number of oscillator shells involved in our calculations runs from zero to $N_{sh,\,\rm max} = 70$. These values of $K_{\rm max}$ and $N_{sh,\,\rm max}$, as was shown in Refs. [40–43], provided fairly good descriptions of bound states and resonance states generated by a three-cluster continuum.

A. ^{7}Li and ^{7}Be

Consider evolution of the ^{7}Li spectrum when we involve more and more hyperspherical harmonics. We consider the $3/2^-$ state in both nuclei. This state is mainly represented by the total orbital momentum $L = 1$. We restrict ourselves to only the value of the total spin $S = 1/2$, and neglect contribution of a negative parity state with total orbital momentum $L = 2$. For the total orbital momentum $L = 1$, we have only odd values of the hypermomentum, $K = 1,3,5\ldots$. Thus we represent results with $K = 1$, $K = 3$, and so on up to $K_{\rm max} = 13$.

Dependence of energy of the $3/2^-$ states in ^{7}Li on quantum number $N_{\rm sh}$ is displayed in Fig. 5. Here we presented trajectories of eigenvalues for ^{7}Li calculated with the hyperspherical harmonics $K_{\rm max} = 7$, $K_{\rm max} = 9$, $K_{\rm max} = 11$, and $K_{\rm max} = 13$. Figure 5 demonstrates rather fast convergence of the ^{7}Li ground-state energy. For the sake of convenience in Fig. 5 we connected all discrete points by lines; however, the results are relevant only for discrete values of $N_{\rm sh}$. Thus we need only a restricted number of hyperspherical harmonics ($K_{\rm max} = 7$) and a small number of hyperradial excitations (or oscillator shells $N_{\rm sh} \leqslant 30$) to obtain the bound state in ^{7}Li, i.e., an eigenstate of the three-cluster compound system which lies below the lowest two-cluster threshold $^4{\rm He} + {}^3{\rm H}$. The first eigenvalue for all values of $K_{\rm max}$ "scans" the two-cluster continuous spectrum with small values of $N_{\rm sh}$ ($\leqslant 5$) and thus represents continuous spectrum states in the $^6{\rm Li} + n$ channel and in the $^4{\rm He} + {}^3{\rm H}$ channel. The second eigenvalue of the three-cluster Hamiltonian for $7 \leqslant K_{\rm max} \leqslant 13$ is able to describe

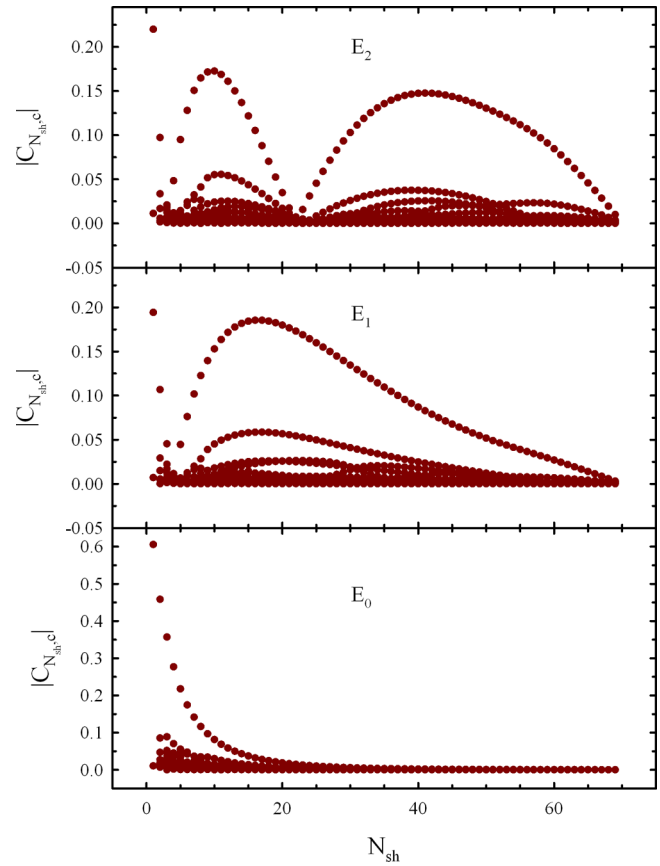

FIG. 6. Wave functions of the $3/2^-$ states in ^{7}Li as a function of $N_{\rm sh}$. These function are presented in the oscillator representation and calculated with $K_{\rm max} = 13$.

continuous spectrum states in the three-cluster continuum and in the binary channels continuum. The larger is the number of hyperspherical harmonics involved in the calculations, the larger is the region of the two-cluster $^4{\rm He} + {}^3{\rm H}$ continuum that can be achieved with these basis functions.

It is important to note that the spectra of ^{7}Li and other nuclei, which will be considered bellow, are obtained by solving the generalized eigenvalue problem represented by Eq. (10). By solving this problem we obtain those states of the compound system which obey the "boundary conditions"

$$C_{n_{\rho,\,\rm max}+1,c} = 0, \tag{23}$$

which are similar to the two-cluster case, considered above. This is demonstrated in Fig. 6, where we display three wave functions of the $3/2^-$ states in ^{7}Li calculated with $K_{\rm max} = 13$. For each value of $N_{\rm sh} \geqslant 7$, there are 56 channels which are involved in construction of all the functions. As we can see, the expansion coefficients tend to zero as $N_{\rm sh}$ approaches its maximal value. We conjecture some important conclusions from this figure. First, we involve a large number of channels c; however, only a few of them dominate in the wave functions of bound and pseudobound states. This result is in agreement with the previous results of the model for the wave functions of the three-cluster continuum (see Refs. [40–43]). In the latter case, such a conclusion was formulated by analyzing

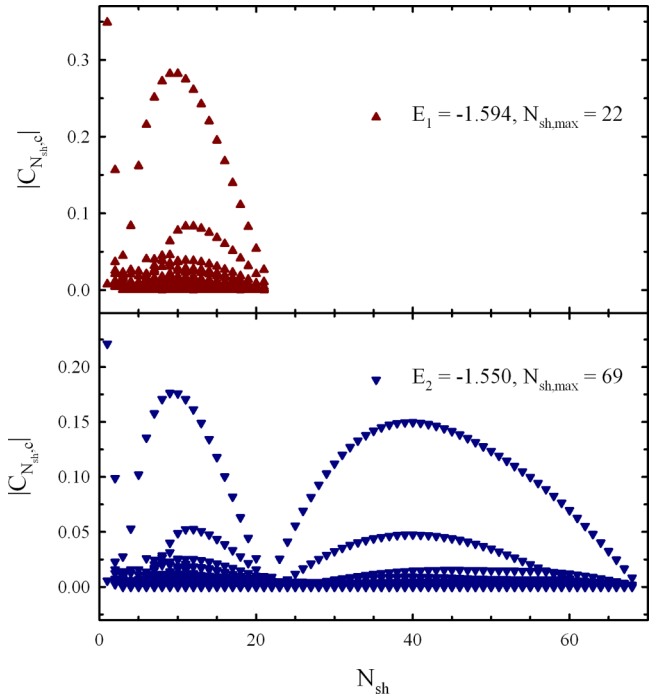

FIG. 7. Comparison of wave functions obtained with the different numbers of oscillator functions but with approximately the same energy.

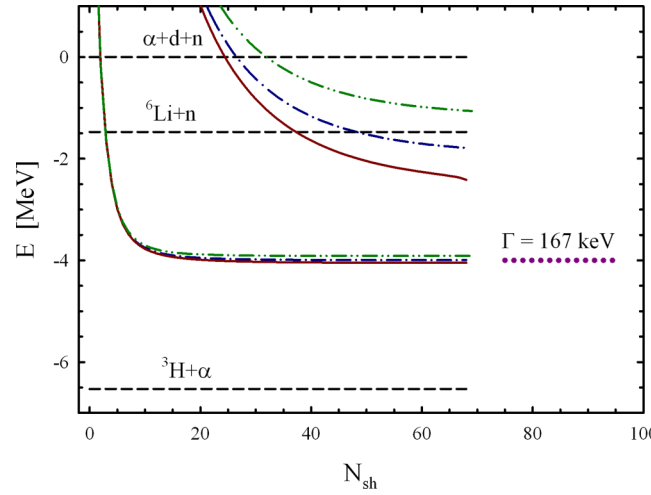

FIG. 8. Spectrum of the $7/2^-$ states in ^{7}Li as a function of $N_{\rm sh}$ calculated with $K_{\rm max} = 9$ (dash-dot-dot lines), $K_{\rm max} = 11$ (dash-dot lines), and $K_{\rm max} = 13$ (solid lines). The dotted line indicates the position of the $7/2^-$ resonance state in ^{7}Li calculated with an alternative microscopical method (see text for details).

the asymptotic part of the wave functions. Second, there is an apparent similarity between the wave functions of two- and three-cluster models, which, for example, exhibits in the number of nodes and in the shape of the wave functions.

Figure 7 demonstrates that wave functions with the same energy but obtained with the different numbers of oscillator functions are similar to each other in the range of smaller values of $N_{\rm sh}$ and differ only by a normalization factor. These wave functions represent $3/2^-$ states of ^{7}Li and are calculated with $K_{\rm max} = 13$. Note that 982 oscillator functions participate in the construction of the first wave function (upper panel), while 3614 oscillator functions are involved in the expansion of the second wave function (lower panel). It is noteworthy that using oscillator functions up to $N_{sh,\,\rm max}$ allows us to describe and to analyze wave functions and intercluster distance in the range $0 \leqslant \rho \leqslant b\sqrt{4N_{sh,\,\rm max} + 2L + 6}$. This inequality reflects a very important feature of oscillator functions. As it is easy to see, the second wave function repeats the behavior of the first wave function in the range $0 \leqslant N_{\rm sh} \leqslant 22$, and represents a new part of the wave function for larger values of $N_{\rm sh}$: $22 < N_{\rm sh} \leqslant 69$.

Figures 6 and 7 demonstrate very interesting properties of wave functions in the oscillator representation. A large number of hyperspherical channels ($N_{ch} = 58$ with $K_{\rm max} = 13$) are involved to calculate the bound and pseudobound states for $J^\pi = 3/2^-$ in ^{7}Li. However, as one can see in Figs. 6 and 7, there is one dominant channel and a few other channels which give noticeable contribution to the wave functions of these states. A large number of channels have very small or negligible contribution to the displayed wave functions.

In Figure 8 we display trajectories of eigenenergies of ^{7}Li for the $7/2^-$ state. These trajectories are calculated with $K_{\rm max} = 9$, $K_{\rm max} = 11$, and $K_{\rm max} = 13$. One can see that the lowest eigenstates have plateaus at energies $E = -3.91$ MeV ($K_{\rm max} = 11$), $E = -3.99$ MeV ($K_{\rm max} = 11$), and $E = -4.05$ MeV ($K_{\rm max} = 13$). These energies are practically stable when we change $N_{\rm sh}$ from 45 to 70. Such plateaus may indicate that there are narrow resonance states at these energies. This is a very simple but reliable way to locate the position of a narrow resonance state which is used in the stabilization method [44]. To be sure, we made use of an alternative method to calculate the energy and width of the resonance state in the two-body continuum. We refer to this method as AMGOB (algebraic model for scattering which involves Gaussian and oscillator basis to describe relative motion of three clusters); it imposes proper boundary conditions for scattering of the third cluster on a bound state of a two-cluster subsystem. This method was formulated in Ref. [7] and applied to study bound and resonance states in ^{7}Be. Investigation of discrete and continuous spectra in ^{7}Li within the AMGOB method was carried out in Ref. [6]. We adopted this model to study resonance states in ^{7}Li with the same input parameters that are used in the AMHHB model. Results of these calculations are shown in Fig. 8 by a dashed line indicating the energy of the $7/2^-$ resonance state. We observe a very good agreement between these two methods. Thus our method (AMHHB), even with a rather restricted basis of hyperspherical functions, correctly predicts the position of the $7/2^-$ resonance state. It is worth emphasizing that the stabilization method works perfectly only for narrow resonance states. This the case for the $7/2^-$ resonance state as its total width is equal to 167 keV.

To understand the essence of the method used and to determine the impact of $K_{\rm max}$ and $N_{\rm sh}$ on the obtained results, we consider the geometry of the three-cluster system $\alpha + d + n$ in the $7/2^-$ states of ^{7}Li. As was demonstrated, three

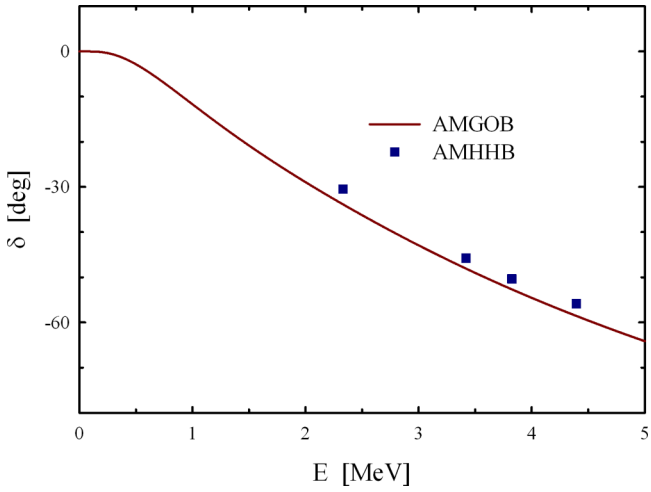

FIG. 9. Phase shift of the $\alpha + t$ scattering calculated within the AMGOB and AMHHB methods. Details are in the text.

approximations with $K_{\max} = 9$, $K_{\max} = 11$, and $K_{\max} = 13$ give very close energies of the lowest $7/2^-$ states. In these cases one can see explicitly and unambiguously the role $K_{\max}$ and $N_{\rm sh}$ in the description of three-cluster nuclei with hyperspherical harmonics. We analyzed wave functions and the density distributions of the resonance states obtained with $K_{\max} = 9$, $K_{\max} = 11$, and $K_{\max} = 13$. It is deduced from this analysis that by increasing the number of channels from $K_{\max} = 9$ to $K_{\max} = 13$ we slightly improve the description of the $t = d + n$ subsystem composing the ^{3}H nucleus. When we increase $N_{\rm sh}$ from minimal to maximal value, we allow a three-cluster system to have larger distance between all clusters or between the third cluster and a compact (i.e., bound) state of a two-cluster subsystem.

In Fig. 9 we compare phase shifts of elastic $\alpha + t$ scattering in the state $J^\pi = 3/2^-$ calculated within AMGOB [6], which represents here the exact phase shift, and evaluated within the present model (AMHHB). We use the approximate way, which follows from Eq. (23) and involves asymptotic behavior of wave function represented by Eq. (16). This approximate way is described in more detail in Ref. [30]. To make such evaluations, one needs to know the energy (with respect to the lowest two-cluster threshold) obtained with diagonalization, the number of oscillator shells involved in calculations, and the expansion coefficients for regular and irregular solutions of the asymptotic Hamiltonian. As we see, the approximate phase shifts calculated with AMHHB are close to the "exact' phase shift. We selected only a few points to demonstrate the ability of such a simple method of phase shift calculations. Unfortunately, the approximate method allows us to calculate phase shift at discrete points and not for all desired energies. Thus one has to implement proper boundary conditions to calculate phase shifts or elements of the S matrix at any energy with acceptable precision. This will be a subject of our next papers.

From the presented figures and from the analysis of wave functions of the states in the two-body continuum we conjecture that as more channels of the hyperspherical harmonics

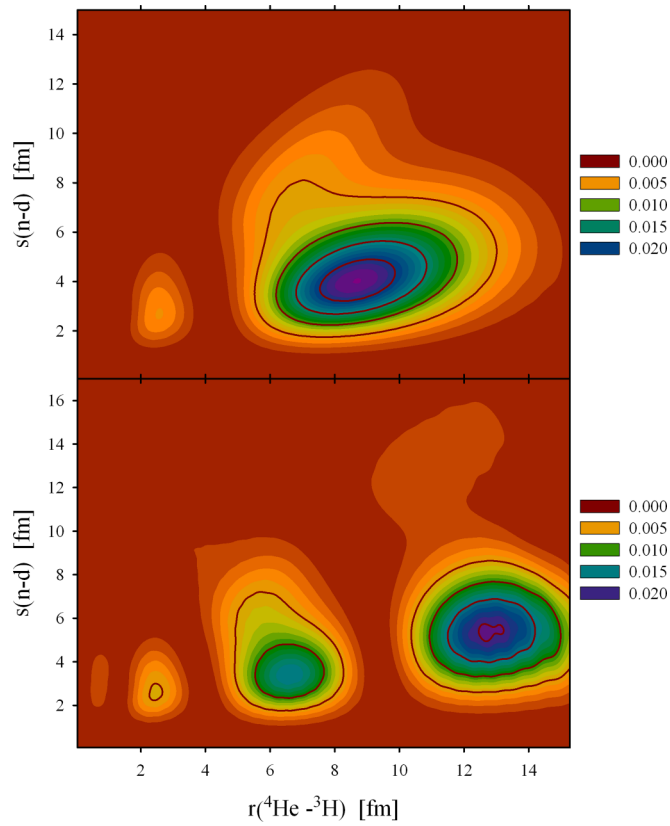

FIG. 10. The correlations functions for the first excited state (upper part) and for the second excited state (lower part) in ^{7}Li.

(or larger values of $K_{\max}$) are involved, the more precise is the description of two-cluster bound states. By increasing $N_{\rm sh}$ with a fixed value of $K_{\max}$, we allow the third cluster to move far away from the bound two-cluster subsystem.

We can determine the most probable shape of the triangle of a three-cluster system by considering wave functions of the ground and excited states in the coordinate or oscillator representations.

Let us consider the correlation functions, which we define as

$$D_{E_\nu}(x_\alpha, y_\alpha) = \sum_{\lambda_\alpha, l_\alpha} \left|\psi^{(\alpha)}_{E_\nu;\lambda_\alpha,l_\alpha;L}(x_\alpha, y_\alpha)\right|^2 x_\alpha^2 y_\alpha^2.$$

For an adequate physical interpretation of the correlation function, we introduce s_α, r_α distances between clusters instead of the Jacobi coordinates x_α, y_α:

$$\mathbf{s}_\alpha = \sqrt{\frac{A_\beta + A_\gamma}{A_\beta A_\gamma}}\mathbf{x}_\alpha, \quad \mathbf{r}_\alpha = \sqrt{\frac{A_\alpha + A_\beta + A_\gamma}{A_\alpha\left(A_\beta + A_\gamma\right)}}\mathbf{y}_\alpha.$$

We will show correlation functions $D_{E_\nu}(s_\alpha, r_\alpha)$ for bound and pseudobound states. We will also display sections of the correlation functions $D_{E_\nu}(s_\alpha, r_{\alpha,\max})$ and $D_{E_\nu}(s_{\alpha,\max}, r_\alpha)$, where $(s_{\alpha,\max}, r_{\alpha,\max})$ is a point in the two-dimensional plane (s_α, r_α) determining a principal maximum of the correlation function for an eigenstate of the three-cluster Hamiltonian with energy E_ν. Coordinates (s_α, r_α) of the principal and local maxima of the correlation function determine maximal

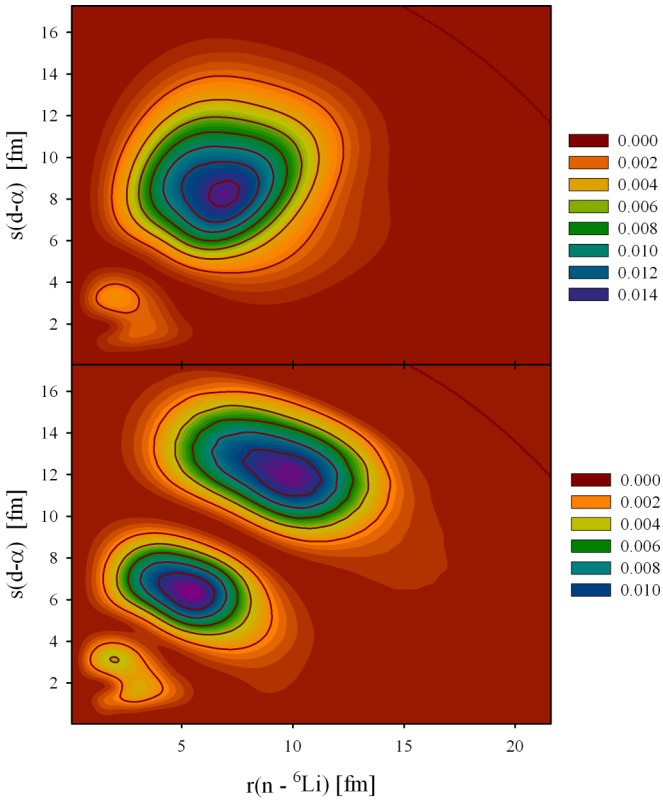

FIG. 11. The correlation functions for the first and second excited states in ^{7}Li obtained for the second Jacobi tree.

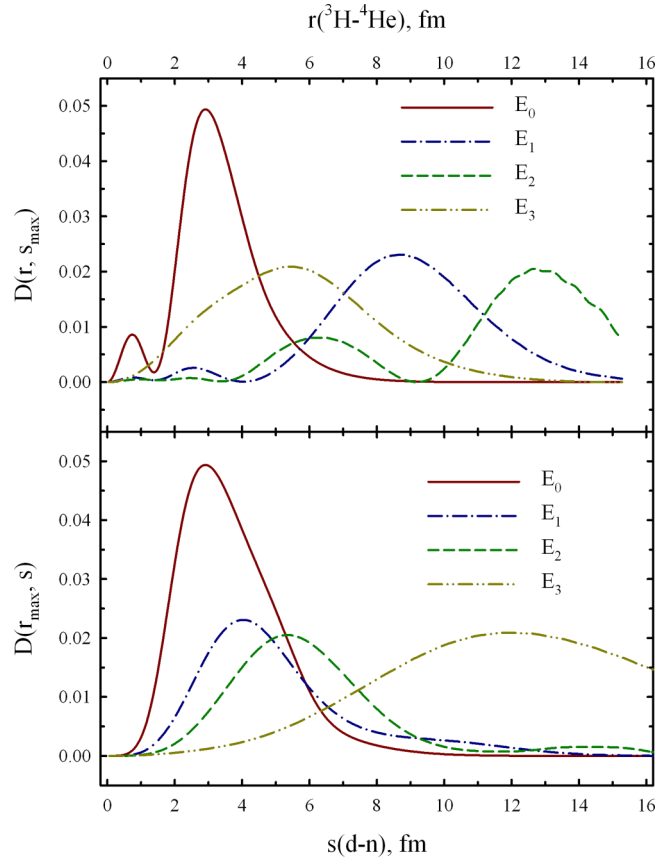

FIG. 12. Parts of the correlation functions for the $J^\pi = 3/2^-$ ground and excited states of ^{7}Li.

probability of finding a three-cluster system at this point, thus we will call them the dominant distances between clusters and we will refer to the quantity s_α as the dominant size of a two-cluster subsystem.

The contour plots of the correlation functions for the first and second excited states in ^{7}Li are presented in Fig. 10. This figure is constructed for the first Jacobi tree, where $\mathbf{s}_1$ determines the distance between neutron and deuteron while vector $\mathbf{r}_1$ represents the distance between an α particle and the ^{3}H nucleus. It is important to recall that both states belong to the ^{4}He + ^{3}H continuum. One may notice that the as the energy of the excited state increases, more oscillations of the correlation functions are observed along the distance r_1 within the presented range. One may also see that the larger is the distance between an α particle and ^{3}H, the larger is the dominant size of ^{3}H or, in other words, the larger is the distance between the deuteron and neutron composing the nucleus ^{3}H. Such behavior of the correlation functions indicates the polarizability of ^{3}H as a two-cluster subsystem when the distance between ^{3}H and the α particle is changed. These results are in accordance with the results of Refs. [6,7], where the cluster polarizabilities of two-cluster subsystems in ^{7}Be and ^{7}Li were investigated with a model designed to study effects of cluster polarization on the structure of bound and resonance states in compound systems.

In the second Jacobi tree with the dominant two-cluster configuration n + ^{6}Li, we obtain a rather different view (Fig. 11) of the correlations functions for the same excited states in ^{7}Li. In this representation, the size of ^{6}Li and distance between the neutron and ^{6}Li nucleus are very large. This is consistent with Fig. 10, where the dominant distance between deuteron and neutron is small, but the dominant distances between neutron and α particle and between deuteron and α particle are very large.

In Fig. 12 we display sections $D_{E_v}(s_\alpha, r_{\alpha,\max})$ and $D_{E_v}(s_{\alpha,\max}, r_\alpha)$ of the correlation functions for the lowest states of ^{7}Li with total angular momentum $J^\pi = 3/2^-$. The lower part of Fig. 12 shows that nucleus ^{3}H, composed of a deuteron and a neutron, is confined in states E_0, E_1, and E_2. With increasing energy, the distance between deuteron and neutron is increased from 3 to 5.5 fm. As in Fig. 10, such behavior of wave functions of ^{3}H in E_0, E_1, and E_2 states more explicitly shows a polarization of the ^{3}H cluster when it interacts with an α particle. The upper part of Fig. 12 demonstrates that ^{7}Li is a compact object in its ground state, since the dominant distance between clusters ^{3}H and ^{4}He is approximately 3 fm. Wave functions and correlation functions of the excited states E_1 and E_2 have an oscillatory behavior along coordinate r_1, determining the distance between clusters ^{3}H and ^{4}He. As one can see in Fig. 5, these states belong to the ^{3}H + ^{4}He continuous spectrum.

The behavior of the presented correlations functions is totally in agreement with the asymptotic forms of three-cluster wave functions discussed above, in Eqs. (16)–(21). Indeed,

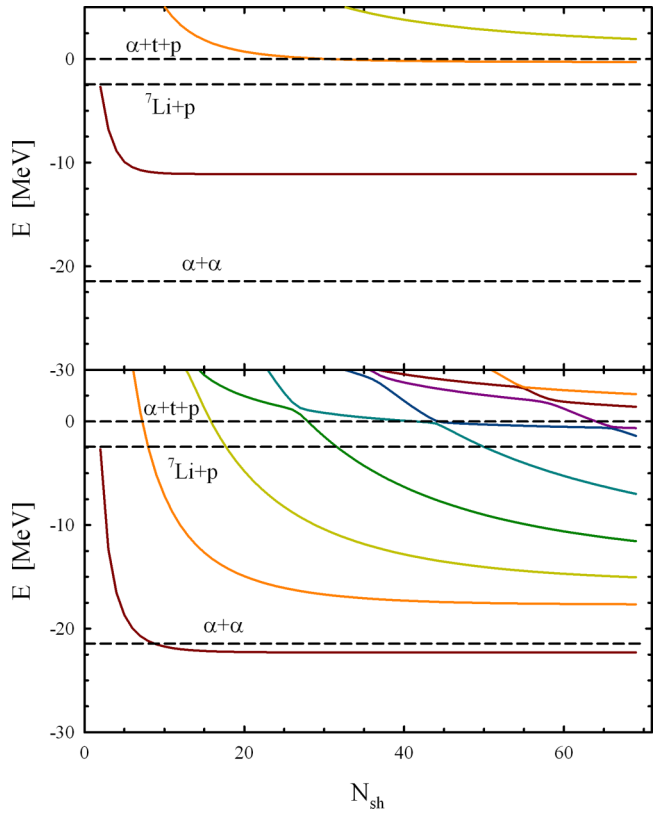

FIG. 13. Spectrum of 0^+ states in ^{8}Be as a function of N_{sh}, calculated with $K_{max} = 0$ (upper part) and $K_{max} = 14$ (lower part of the figure).

for the bound state we observe the exponential tails of the correlation functions along the vectors $\mathbf{s}_\alpha$ and $\mathbf{r}_\alpha$, while for the states in the two-body continuum the exponential tail is observed along the vector $\mathbf{s}_\alpha$ and the oscillating tail is seen along the vector $\mathbf{r}_\alpha$. These conclusions are correct not only for ^{7}Li but also for all other nuclei considered in this paper.

Concluding this section, we note that we have carried out similar investigations for the mirror nucleus ^{7}Be as a three-cluster configuration, $^7\text{Be} = \alpha + d + p$. The Coulomb interaction, which is stronger in ^{7}Be, slightly changes the energy of the two-cluster threshold $^4\text{He} + {}^3\text{He}$ and reduces the energy of the ^{7}Be ground state with respect to two- and three-cluster thresholds. Therefore, all results and conclusions deduced for the ^{7}Li nucleus are valid for the mirror nucleus. Due to lack of room in the present paper, we will not dwell on the results for ^{7}Be.

B. $^8\text{Be} = {}^4\text{He} + {}^3\text{H} + p$

Now we consider spectrum and wave functions of the 0^+ state in ^{8}Be. With the three-cluster configuration $^4\text{He} + {}^3\text{H} + p$ we have the binary channels $^4\text{He} + {}^4\text{He}$ and $^7\text{Li} + p$. We do not consider the binary channel $^5\text{Li} + {}^3\text{H}$ as its threshold energy exceeds the three-cluster threshold. The energy of 0^+ states in ^{8}Be, calculated with only one hyperspherical harmonic $K = 0$ and with $K_{max} = 14$, as a function of N_{sh} is displayed in Fig. 13. The first and important result is that

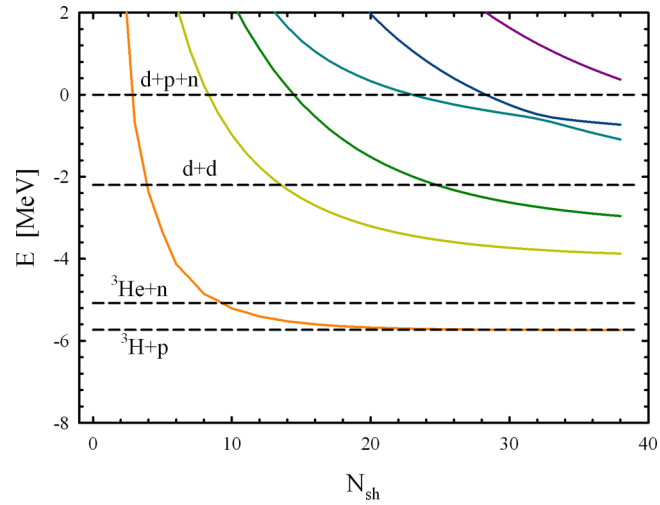

FIG. 14. Spectrum of the 0^+ state in ^{4}He calculated with $K_{max} = 14$.

only one hyperspherical harmonic ($K = 0$) is able to produce one state in the $^4\text{He} + {}^4\text{He}$ continuum and one state above the $^7\text{Li} + p$ threshold but below the three-cluster $^4\text{He} + {}^3\text{H} + p$ threshold. Besides, the "ground" 0^+ state appears in the two-cluster $^4\text{He} + {}^4\text{He}$ continuum starting with $N_{sh} = 2$, while the first excited state needs more than $N_{sh} = 30$ oscillator shells to appear in the $^7\text{Li} + p$ continuum. It is interesting to note (see the lower part of Fig. 13) that hyperspherical harmonics with $K_{max} = 14$ generate one bound state (below the $^4\text{He} + {}^4\text{He}$ threshold) and four states in the two-cluster $^4\text{He} + {}^4\text{He}$ continuum and also two states in the $^7\text{Li} + p$ continuum. Thus this number of hyperspherical harmonics (i.e., all harmonics with $0 \leqslant K \leqslant 14$ or 36 channels) is able to describe some states of elastic $^4\text{He} + {}^4\text{He}$ and $^7\text{Li} + p$ scattering and the reaction $^4\text{He} + {}^4\text{He} \Longleftrightarrow {}^7\text{Li} + p$ at two discrete energy points. It should be stressed that these results are obtained without imposing boundary conditions.

C. $^4\text{He} = d + p + n$

We consider ^{4}He as a three-cluster configuration $^4\text{He} = d + p + n$. This configuration allows us to take into account all binary channels of ^{4}He, namely, $^3\text{H} + p$, $^3\text{He} + n$, and $d + d$. Besides, this configuration allows us to describe more correctly

TABLE III. Energies of the ground and the lowest excited 0^+ states in ^{10}Be. Dominant two-body channels and their threshold energies E_{th} are also presented.

Two-cluster threshold	E (MeV)
	−9.162
	−2.197
$^6\text{He} + \alpha$	$E_{th} = -1.745$
	−0.343
$^8\text{Be} + 2n$	$E_{th} = -0.023$
	0.561
	1.162

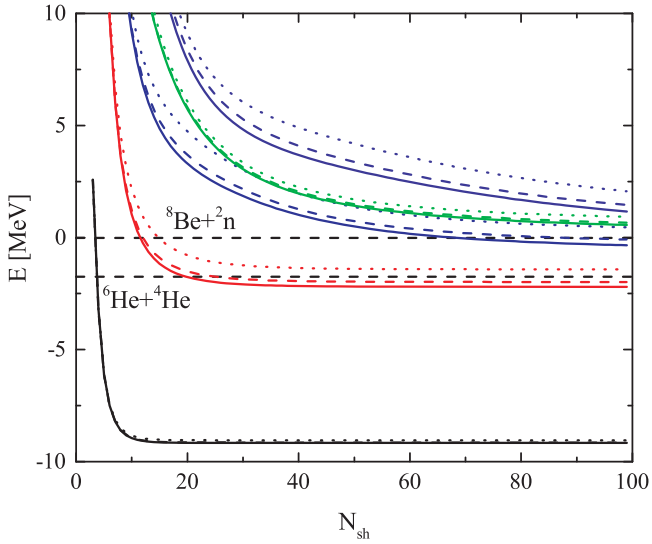

FIG. 15. Spectrum of the 0^+ states in ^{10}Be as a function of $N_{\rm sh}$ and $K_{\rm max}$. Dotted lines correspond to $K_{\rm max} = 6$, dashed lines denote $K_{\rm max} = 10$, and solid lines stand for $K_{\rm max} = 14$.

the internal structure of clusters ^{3}H and ^{3}He, which are treated as two-cluster systems $d + n$ and $d + p$, respectively. The trajectories of eigenstates of ^{4}He are displayed in Fig. 14. They are obtained with $K_{\rm max} = 14$. These eigenstates scan continuous spectrum above the ^{3}H + p, ^{3}He + n, and $d + d$

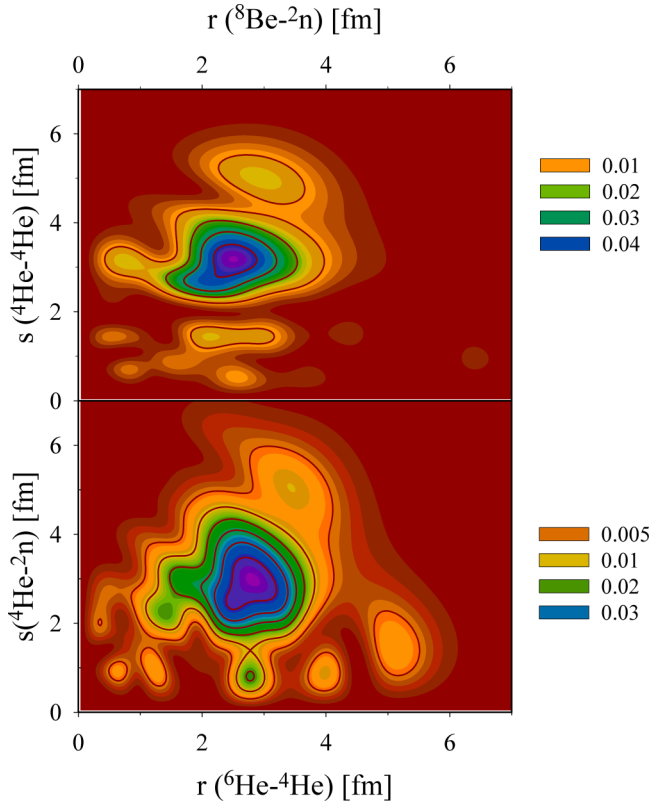

FIG. 16. The correlation functions for the ground state in ^{10}Be in different Jacobi trees.

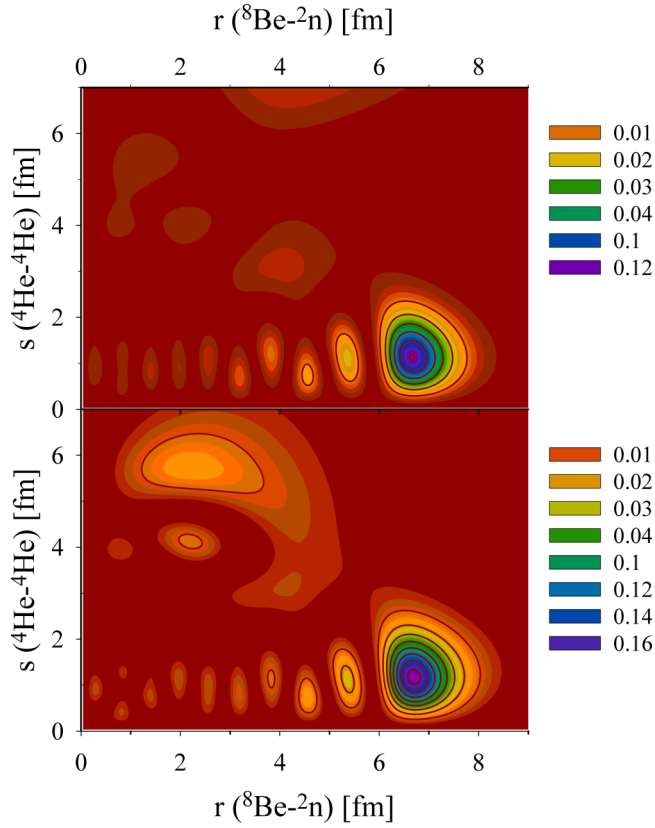

FIG. 17. The correlation functions for the first excited state (lower part) and for the second excited state (upper part) in ^{10}Be.

thresholds. We do not display the ground state of ^{4}He which lies 20 MeV below the ^{3}H + p thresholds. Being deeply bound, the ground states require a very small number of hyperspherical harmonics and a very restricted number of hyperradial excitations.

D. ^{10}Be

Let us consider spectrum of ^{10}Be, provided that ^{10}Be is treated as a $\alpha + \alpha + 2n$ three-cluster configuration, and analyze what is the most probable geometry of this three-cluster structure. In Table III we show the ground and the first excited 0^+ states in ^{10}Be. The results are obtained with the MP. In Ref. [8] the exchange parameter u of the potential was selected so as to reproduce the energy of the ^{10}Be ground state with respect to the binary threshold ^{6}He + α. We use the same value of this parameter. With this value of the parameter u we obtained the relative position of the threshold energies of the binary ^{6}He + α and ^{8}Be + $2n$ channels indicated in Table III.

As can be seen from Table III, the ground state and the first excited 0^+ state are below the lowest binary decay threshold of ^{10}Be. The second excited state lies between ^{6}He + α and ^{8}Be + $2n$ thresholds, while the rest of the states belong to the three-cluster continuum.

The spectrum of the 0^+ states in ^{10}Be as a function of the number of oscillator shells and the maximum value of hypermomentum involved in the calculations are plotted in Fig. 15. As is evident from Fig. 15, to reproduce the energy

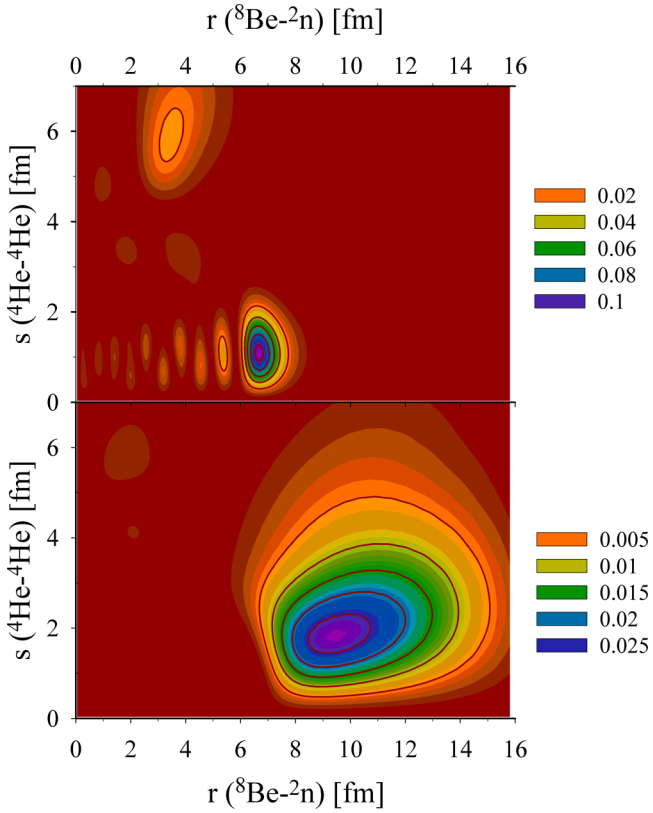

FIG. 18. The correlation functions for the third excited state (lower part) and for the fourth excited state (upper part) in ^{10}Be.

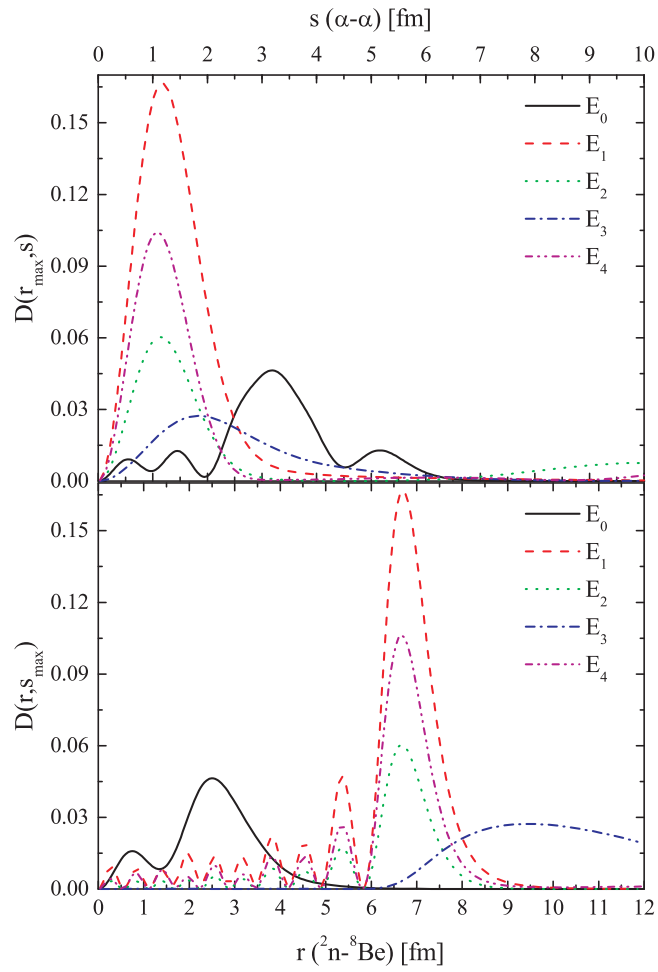

FIG. 19. Parts of the correlation functions for the $J^\pi = 0^+$ ground and excited states of ^{10}Be.

of the ground state it is sufficient to invoke basis functions with $N_{\rm sh} = 20$ and $K_{\rm max} = 6$. For increasing energy of the state, larger values of the number of oscillator shells and hypermomentum should be used to reach convergence. However, the third excited state with energy $E = 0.56$ MeV above the three-cluster decay threshold of ^{10}Be somewhat differs from the other states presented in Fig. 15. Hyperharmonics with $K_{\rm max} \geqslant 10$ slightly contribute to the energy of this state as opposed to the neighboring excited states.

Figures 16, 17, and 18 display contour plots of the correlation functions for the ground and excited states in ^{10}Be tabulated in Table III. Referring to Fig. 16, we can conclude that ^{10}Be in its ground state is a system of three equally spaced clusters (two α particles and a dineutron). The other four excited states, contrastingly, have prominent $^8\mathrm{Be} + 2n$ structure, as is clear from Figs. 17 and 18. The $^6\mathrm{He} + \alpha$ configuration reveals itself only at higher energies.

Sections of the correlation functions presented in Figs. 16, 17, and 18 are shown in Fig. 19. As may be inferred from Fig. 19, in three low-lying states of ^{10}Be the ^{8}Be subsystem is rather compact compared to the distance between ^{8}Be and a dineutron. The first state above the three-cluster decay threshold is characterized by a somewhat more dilute ^{8}Be subsystem, but the $^8\mathrm{Be} + 2n$ configuration still dominates in this state.

We did not consider in detail the convergence that the present model provides for the bound states in the selected nuclei. However, some conclusions can be made from Fig. 5, where we display the spectrum of the $3/2^-$ states in ^{7}Li calculated with different values of $K_{\rm max}$ and $N_{\rm sh}$. To demonstrate that the present model provides us with a satisfactory description of the bound states, in Fig. 20 we show the ground-state energies of ^{7}Li and ^{7}Be and the energies of the ground and first excited 0^+ states in ^{10}Be. We compare results of the present model with the corresponding results of the AMGOB model mentioned above. The AMGOB model involves a little larger part of the total Hilbert space to describe the discrete and continuous spectrum of a three-cluster system, which is reduced to a set of binary channels. In Refs. [6–8] the AMGOB model was applied to study nuclei ^{7}Li, ^{7}Be, and ^{10}Be with the same input parameters that we use in the present model. Therefore, we will consider results of the model as "exact." In Fig. 20 we also display by dashed lines both the three-cluster and the lowest two-cluster thresholds. We can see that all ground states are deeply bound states with respect to the three-cluster threshold; however, their convergence strongly depends on how far these states lie with respect to the lowest two-cluster channel. The latter, as we pointed above, determines the shape of the asymptotic part of the bound-state wave function. As one could expect, the Coulomb interaction reduces the bound-state energy in ^{7}Be (comparing to ^{7}Li) and slows down the

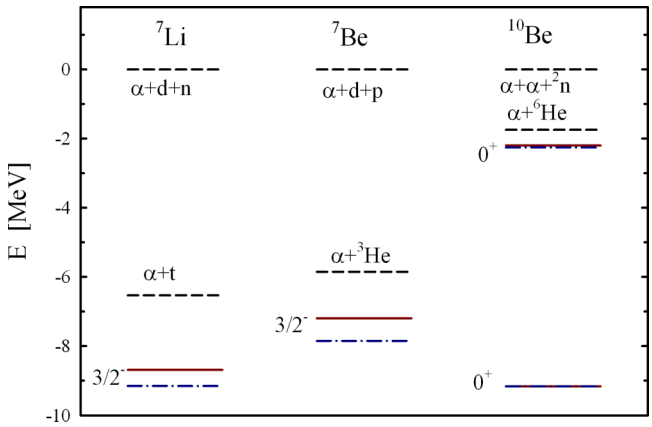

FIG. 20. Energies of the $3/2^-$ ground states in ^{7}Li and ^{7}Be, and the ground and first excited 0^+ states in ^{10}Be calculated within the present model (solid line) and within the AMGOB model (dash-dotted line).

convergence of this state. In conclusion, the presented results show that our model is able to reproduce the bound-state energy of the considered nuclei with a satisfactory precision.

IV. CONCLUSION

Within a microscopic three-cluster model we have considered spectra of a set of light nuclei: ^{4}He, ^{7}Li, ^{7}Be, ^{8}Be, and ^{10}Be. We selected nuclei that have a dominant three-cluster channel and one or more two-body channels below the three-cluster decay threshold. We considered three kinds of nuclei. Two of these nuclei are deeply bound (^{4}He and ^{10}Be), as their ground states lie below -8 MeV with respect to the lowest two-cluster threshold. Two other nuclei (^{7}Li and ^{7}Be) are weekly bound, since their binding energies do not exceed -2.6 MeV. The last nucleus ^{8}Be has no bound states. A full set of the antisymmetric three-cluster oscillator functions was constructed. These functions were labeled by the quantum numbers of the hyperspherical harmonics method. Matrix elements of a Hamiltonian, consisting of central nucleon-nucleon forces and the Coulomb potential, between the oscillator functions were constructed and eigenvalues and corresponding eigenfunctions were calculated. We analyzed dependence of the eigenvalues on the number of oscillator functions involved in calculations. It was demonstrated that some of the eigenvalues are discrete states in the two-cluster continuum. Analysis of the wave functions in coordinate and oscillator representations showed that these functions have a correct asymptotic behavior peculiar to the two-cluster continuous spectrum.

The main result of the present investigations is that it is possible to see the evidence of two-cluster structure in the three-cluster wave function of a pseudobound state, but with a rather restricted set of hyperspherical harmonics and hyperradial excitations as well. It was demonstrated that the eigenstates of the three-cluster Hamiltonian have correct asymptotic behavior both for bound states below the two-cluster threshold and states in the two-cluster continuum. Analysis of the correlation functions in different Jacobi trees reveals polarizability of two-cluster bound states when the distance between the third cluster and two-cluster subsystem is relatively small.

ACKNOWLEDGMENTS

This work was supported in part by the Program of Fundamental Research of the Physics and Astronomy Department of the National Academy of Sciences of Ukraine (Project No. 0117U000239) and by the Ministry of Education and Science of the Republic of Kazakhstan, Research Grant No. IPS 3106/GF4.

[1] F. Aguila and M. G. Doncel, Nuovo Cimento A **59**, 283 (1980).
[2] O. V. Bochkarev, L. V. Chulkov, A. A. Korsheninnikov, E. A. Kuz'min, I. G. Mukha, and G. B. Yankov, Nucl. Phys. A **505**, 215 (1989).
[3] R. J. Charity, K. Mercurio, L. G. Sobotka, J. M. Elson, M. Famiano, A. Banu, C. Fu, L. Trache, and R. E. Tribble, Phys. Rev. C **75**, 051304 (2007).
[4] R. I. Jibuti and R. Y. Keserashvili, Czech. J. Phys. **30**, 1090 (1980).
[5] E. Gerjuoy, Philos. Trans. R. Soc. London A **270**, 197 (1971).
[6] A. V. Nesterov, V. S. Vasilevsky, and T. P. Kovalenko, Phys. At. Nucl. **72**, 1450 (2009).
[7] V. S. Vasilevsky, F. Arickx, J. Broeckhove, and T. P. Kovalenko, Nucl. Phys. A **824**, 37 (2009).
[8] Y. A. Lashko, G. F. Filippov, and V. S. Vasilevsky, Nucl. Phys. A **958**, 78 (2017).
[9] D. R. Tilley, C. M. Cheves, J. L. Godwin, G. M. Hale, H. M. Hofmann, J. H. Kelley, C. G. Sheu, and H. R. Weller, Nucl. Phys. A **708**, 3 (2002).
[10] T. K. Das, H. T. Coelho, and M. Fabre de la Ripelle, Phys. Rev. C **26**, 2288 (1982).
[11] J. L. Ballot, M. Fabre de la Ripelle, and J. S. Levinger, Phys. Rev. C **26**, 2301 (1982).
[12] E. Nielsen, D. V. Fedorov, A. S. Jensen, and E. Garrido, Phys. Rep. **347**, 373 (2001).
[13] K. M. Daily, A. Kievsky, and C. H. Greene, Few-Body Syst. **56**, 753 (2015).
[14] V. Vasilevsky, A. V. Nesterov, F. Arickx, and J. Broeckhove, Phys. Rev. C **63**, 034606 (2001).
[15] F. Zernike and H. C. Brinkman, Proc. Kon. Acad. Wetensch. Amsterdam **38**, 161 (1935).
[16] M. V. Zhukov, B. V. Danilin, D. V. Fedorov, J. M. Bang, I. J. Thompson, and J. S. Vaagen, Phys. Rep. **231**, 151 (1993).
[17] M. Viviani, A. Kievsky, and S. Rosati, Few-Body Sys. **30**, 39 (2001).
[18] C. R. Chen, J. L. Friar, and G. L. Payne, Few-Body Sys. **31**, 13 (2001).,
[19] V. Vasilevsky, A. V. Nesterov, F. Arickx, and J. Broeckhove, Phys. Rev. C **63**, 034607 (2001).

[20] A. V. Nesterov, F. Arickx, J. Broeckhove, and V. S. Vasilevsky, Phys. Part. Nucl. **41**, 716 (2010).
[21] S. Korennov and P. Descouvemont, Nucl. Phys. A **740**, 249 (2004).
[22] V. S. Vasilevsky, A. V. Nesterov, F. Arickx, and P. van Leuven, Yad. Fiz. **60**, 413 (1997) [Phys. Atomic Nuclei **60**, 343 (1997)].
[23] V. S. Vasilevsky, A. V. Nesterov, and O. F. Chernov, Phys. At. Nucl. **64**, 1409 (2001).
[24] S. P. Merkuriev, C. Gignoux, and A. Laverne, Ann. Phys. (N.Y.) **99**, 30 (1976).
[25] L. D. Faddeev and S. P. Merkuriev, *Quantum Scattering Theory for Several Particle Systems* (Kluwer, Dordrecht, 1993).
[26] J. L. Friar and G. L. Payne, in *Coulomb Interactions in Nuclear and Atomic Few-Body Collisions*, edited by F. S. Levin and D. A. Micha (Plenum, New York, 1996), pp. 97–168.
[27] G. F. Filippov and I. P. Okhrimenko, Yad. Fiz. **32**, 932 (1980) [Sov. J. Nucl. Phys. **32**, 480 (1980)].
[28] G. F. Filippov, Yad. Fiz. **33**, 928 (1981) [Sov. J. Nucl. Phys. **33**, 488 (1981)].
[29] E. J. Heller and H. A. Yamani, Phys. Rev. A **9**, 1201 (1974).
[30] G. F. Filippov, L. L. Chopovsky, and V. S. Vasilevsky, Yad. Fiz. **37**, 839 (1981) [Sov. J. Nucl. Phys. **37**, 500 (1983)].
[31] G. F. Filippov and Yu. A. Lashko, Fiz. Elem. Chastits At. Yadra **36**, 1373 (2005) [Phys. Part. Nuclei **36**, 714 (2005)].
[32] *The J-Matrix Method. Developments and Applications*, edited by A. D. Alhaidari, H. A. Yamani, E. J. Heller, and M. S. Abdelmonem (Springer, Dordrecht, 2008).
[33] H. A. Yamani and L. Fishman, J. Math. Phys. **16**, 410 (1975).
[34] T. Y. Mikhelashvili, A. M. Shirokov, and Y. F. Smirnov, J. Phys. G Nucl. Phys. **16**, 1241 (1990).
[35] S. A. Zaitsev, Y. F. Smirnov, and A. M. Shirokov, Theor. Math. Phys. **117**, 1291 (1998).
[36] T. Myo, Y. Kikuchi, H. Masui, and K. Katō, Progr. Part. Nucl. Phys. **79**, 1 (2014).
[37] H. Horiuchi, K. Ikeda, and K. Katō, Progr. Theor. Phys. Suppl. **192**, 1 (2012).
[38] D. R. Thompson, M. LeMere, and Y. C. Tang, Nucl. Phys. A **286**, 53 (1977).
[39] I. Reichstein and Y. C. Tang, Nucl. Phys. A **158**, 529 (1970).
[40] V. Vasilevsky, A. V. Nesterov, F. Arickx, and J. Broeckhove, Phys. Rev. C **63**, 064604 (2001).
[41] J. Broeckhove, F. Arickx, P. Hellinckx, V. S. Vasilevsky, and A. V. Nesterov, J. Phys. G Nucl. Phys. **34**, 1955 (2007).
[42] V. Vasilevsky, F. Arickx, W. Vanroose, and J. Broeckhove, Phys. Rev. C **85**, 034318 (2012).
[43] V. S. Vasilevsky, K. Katō, and N. Z. Takibayev, Phys. Rev. C **96**, 034322 (2017).
[44] A. U. Hazi and H. S. Taylor, Phys. Rev. A **1**, 1109 (1970).